High-Impedance Electromagnetic Surfaces with a Forbidden Frequency Band

Dan Sievenpiper, *Member, IEEE,* Lijun Zhang, Romulo F. Jimenez Broas, Nicholas G. Alexópolous, *Fellow, IEEE,* and Eli Yablonovitch, *Fellow, IEEE*

***Abstract*— A new type of metallic electromagnetic structure has been developed that is characterized by having high surface impedance. Although it is made of continuous metal, and conducts dc currents, it does not conduct ac currents within a forbidden frequency band. Unlike normal conductors, this new surface does not support propagating surface waves, and its image currents are not phase reversed. The geometry is analogous to a corrugated metal surface in which the corrugations have been folded up into lumped-circuit elements, and distributed in a two-dimensional lattice. The surface can be described using solid-state band theory concepts, even though the periodicity is much less than the free-space wavelength. This unique material is applicable to a variety of electromagnetic problems, including new kinds of low-profile antennas.**

***Index Terms*— Antennas, corrugated surfaces, photonic bandgap, surface impedance, surface waves, textured surfaces.**

I. Introduction

A. Electric Conductors

A FLAT METAL sheet is used in many antennas as a reflector or ground plane [1]. The presence of a ground plane redirects one-half of the radiation into the opposite direction, improving the antenna gain by 3 dB, and partially shielding objects on the other side. If the antenna is too close to the conductive surface, the image currents cancel the currents in the antenna, resulting in poor radiation efficiency. This problem is often addressed by including a quarter-wavelength space between the radiating element and the ground plane, but such a structure then requires a minimum thickness of $\lambda/4$.

Another property of metals is that they support surface waves [2], [3]. These are propagating electromagnetic waves that are bound to the interface between metal and free space. They are called surface plasmons at optical frequencies [4], but at microwave frequencies, they are nothing more than the normal currents that occur on any electric conductor. If the metal surface is smooth and flat, the surface waves will not couple to external plane waves. However, they will radiate vertically if scattered by bends, discontinuities, or surface texture.

Manuscript received March 8, 1999; revised July 9, 1999. This work was supported by the Army Research Office under Grant DAAH04-96-1-0389, by HRL Laboratories under Subcontract S1-602680-1, and by the Office of Naval Research under Grant N00014-99-1-0136.

D. Sievenpiper is with HRL Laboratories, Malibu, CA 90265 USA.

L. Zhang, R. F. J. Broas, and E. Yablonovitch are with the Electrical Engineering Department, University of California at Los Angeles, Los Angeles, CA 90095 USA.

N. G. Alexópolous is with the Department of Electrical and Computer Engineering, University of California at Irvine, Irvine, CA 92697 USA.

Publisher Item Identifier S 0018-9480(99)08780-3.

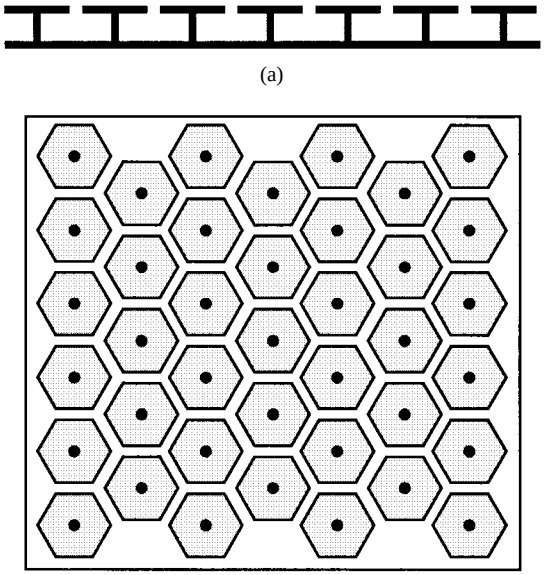

(a)

(b)

Fig. 1. (a) Cross section of a high-impedance surface, fabricated as a printed circuit board. The structure consists of a lattice of metal plates, connected to a solid metal sheet by vertical conducting vias. (b) Top view of the high-impedance surface, showing a triangular lattice of hexagonal metal plates.

Surface waves appear in many situations involving antennas. On a finite ground plane, surface waves propagate until they reach an edge or corner, where they can radiate into free space. The result is a kind of multipath interference or "speckle," which can be seen as ripples in the radiation pattern. Moreover, if multiple antennas share the same ground plane, surface currents can cause unwanted mutual coupling.

B. High-Impedance Surfaces

By incorporating a special texture on a conducting surface, it is possible to alter its radio-frequency electromagnetic properties [5], [6]. In the limit where the period of the surface texture is much smaller than the wavelength, the structure can be described using an effective medium model, and its qualities can be summarized into a single parameter: the surface impedance. A smooth conducting sheet has low surface impedance, but with a specially designed geometry, a textured surface can have high surface impedance.

An example of a high-impedance surface, shown in Fig. 1, consists of an array of metal protrusions on a flat metal sheet.

They are arranged in a two-dimensional lattice, and can be visualized as mushrooms or thumbtacks protruding from the surface. The structure is easily fabricated using printed-circuit-board technology. The protrusions are formed as metal patches on the top surface of the board, connected to the solid lower conducting surface by metal plated vias.

If the protrusions are small compared to the operating wavelength, their electromagnetic properties can be described using lumped-circuit elements—capacitors and inductors. They behave as a network of parallel resonant LC circuits, which act as a two-dimensional electric filter to block the flow of currents along the sheet. In the frequency range where the surface impedance is very high, the tangential magnetic field is small, even with a large electric field along the surface. Such a structure is sometimes described as a "magnetic conductor."

Due to this unusual boundary condition, the high-impedance surface can function as a unique new type of ground plane for low-profile antennas. The image currents are in-phase, rather than out-of-phase, allowing radiating elements to lie directly adjacent to the surface, while still radiating efficiently. For example, a dipole lying flat against a high-impedance ground plane is not shorted out as it would be on an ordinary metal sheet. Furthermore, in a forbidden frequency band, the high-impedance ground plane does not support propagating surface waves, thus, the radiation pattern is typically smooth, and free from the effects of multipath interference along the ground plane.

II. Surface Waves

Surface waves can occur on the interface between two dissimilar materials, such as metal and free space. They are bound to the interface, and decay exponentially into the surrounding materials. At radio frequencies, the fields associated with these waves can extend thousands of wavelengths into the surrounding space, and they are often best described as surface currents. They can be modeled from the viewpoint of an effective dielectric constant, or an effective surface impedance.

A. Dielectric Interfaces

To derive the properties of surface waves on a dielectric interface [3], [7], begin with a surface in the YZ plane, as shown in Fig. 2. The region $X > 0$ is filled with vacuum, while the region $X < 0$ is filled with dielectric ε. Assume a wave that is bound to the surface, decaying in the $+X$-direction with decay constant α, and in the $-X$-direction with decay constant γ. The wave propagates in the Z-direction with propagation constant k. For a TM polarized surface wave, $E_y = 0$. The electric field in the upper half-space has the following form:

$$E_1 = (\hat{x}E_{1x} + \hat{z}E_{1z})e^{j\omega t - jkz - \alpha x}. \tag{1}$$

In the lower half-space, the electric field has a similar form as follows:

$$E_2 = (\hat{x}E_{2x} + \hat{z}E_{2z})e^{j\omega t - jkz + \gamma x}. \tag{2}$$

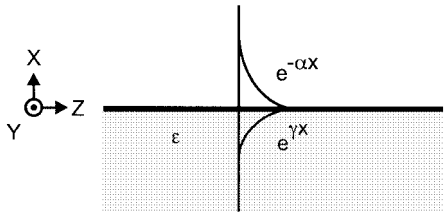

Fig. 2. Surface wave bound to a dielectric interface, decaying exponentially away from the surface.

For the waves described above, Maxwell's equations can be solved to obtain the following results [7]:

$$k = \sqrt{\frac{\varepsilon}{1+\varepsilon}}\frac{\omega}{c} \tag{3}$$

$$\alpha = \sqrt{\frac{-1}{1+\varepsilon}}\frac{\omega}{c} \tag{4}$$

$$\gamma = \sqrt{\frac{-\varepsilon^2}{1+\varepsilon}}\frac{\omega}{c}. \tag{5}$$

If ε is positive, then α and γ are imaginary, and the waves do not decay with distance from the surface; they are simply plane waves propagating through the dielectric interface. Thus, TM surface waves do not exist on nonconductive dielectric materials. On the other hand, if ε is less than -1, or if it is imaginary, the solution describes a wave that is bound to the surface. These TM surface waves can occur on metals, or other materials with nonpositive dielectric constants. The solution for TE surface waves can also be obtained from the foregoing analysis by the principle of duality [1]. If the electric and magnetic fields are exchanged, and μ is substituted for ε, the solution above can be applied to the TE case.

B. Metal Surfaces

The effective, relative dielectric constant of a metal can be expressed in the following form [7]:

$$\varepsilon = 1 - \frac{j\sigma}{\omega\varepsilon_0} \tag{6}$$

σ is the conductivity, which is given by the following equation:

$$\sigma = \frac{nq^2\tau/m}{1 + j\omega\tau} \tag{7}$$

τ is the mean electron collision time, q is the electron charge, and m and n are the effective mass and the density, respectively, of the conduction electrons.

For frequencies much lower than $1/\tau$, including the microwave spectrum, the conductivity is primarily real, and much greater than unity, thus, the dielectric constant is a large imaginary number. Inserting (6) into (3) leads to a simple dispersion relation for surface waves at radio frequencies as follows:

$$k \approx \frac{\omega}{c}. \tag{8}$$

Thus, surface waves propagate at nearly the speed of light in vacuum, and they travel for many wavelengths along the metal surface with little attenuation. By inserting (6) into (4), we can

find the following expression for α, the decay constant of the fields into the surrounding space:

$$\alpha \approx \frac{\omega}{c}\sqrt{\frac{\omega\varepsilon_0}{2\sigma}}(1-j). \tag{9}$$

For good conductors at microwave frequencies, the surface waves extend a great distance into the surrounding space. For example, on a copper surface, the electromagnetic fields associated with a 10-GHz surface wave extend about 70 m, or 2300 wavelengths into free space. Hence, at microwave frequencies they are often described simply as surface currents, rather than surface waves. These surface currents are nothing more than the normal alternating currents that can occur on any conductor.

We can also determine γ, the surface-wave penetration depth into the metal. By inserting (6) into (5), we obtain the following:

$$\gamma \approx (1+j)\sqrt{\frac{\omega\mu_0\sigma}{2}} = \frac{(1+j)}{\delta}. \tag{10}$$

Thus, we have derived the skin depth δ from the surface-wave penetration depth [2]. The surface currents penetrate only a very small distance into the metal. For example, at 10 GHz, the skin depth of copper is less than 1 μm.

From the skin depth, we can derive the surface impedance of a flat metal sheet [3]. Using (10), we can express the current in terms of the skin depth, assuming E_0 is the electric field at the surface

$$J_z(x) = \sigma E_z(x) = \sigma E_0 e^{-x(1+j)/\delta}. \tag{11}$$

The magnetic field at the surface is found by integrating along a path surrounding the thin surface layer of current, extending far into the metal beyond the skin depth as follows:

$$H_0 = \int_0^{-\infty} J_z(x)\,dx = \frac{\sigma\delta}{1+j}E_0. \tag{12}$$

Thus, the surface impedance of a flat sheet of metal is derived as follows:

$$Z_s = \frac{E_z}{H_y} = \frac{1+j}{\sigma\delta}. \tag{13}$$

The surface impedance has equal positive real and positive imaginary parts, so the small surface resistance is accompanied by an equal amount of surface inductance. For example, the surface impedance of copper at 10 GHz is $0.03(1+j)\ \Omega/\square$.

C. High-Impedance Surfaces

By applying a texture to the metal surface, we can alter its surface impedance, and thereby change its surface-wave properties. The behavior of surface waves on a general impedance surface is derived in several electromagnetics textbooks [2], [3]. The derivation proceeds by assuming a wave that decays exponentially away from a boundary, with decay constant α. The boundary is characterized by its surface impedance. It can be shown that TM waves occur on an inductive surface, in which the surface impedance is given by the following expression:

$$Z_s(\mathrm{TM}) = \frac{j\alpha}{\omega\varepsilon}. \tag{14}$$

Conversely, TE waves can occur on a capacitive surface, with the following impedance:

$$Z_s(\mathrm{TE}) = \frac{-j\omega\mu}{\alpha}. \tag{15}$$

The surface impedance of the textured metal surface described in this paper is characterized by an equivalent parallel resonant LC circuit. At low frequencies it is inductive, and supports TM waves. At high frequencies it is capacitive, and supports TE waves. Near the LC resonance frequency, the surface impedance is very high. In this region, waves are not bound to the surface; instead, they radiate readily into the surrounding space.

III. Textured Surfaces

The concept of suppressing surface waves on metals is not new. It has been done before using several geometries, such as a metal sheet covered with small bumps [8], [9], or a corrugated metal slab [11]–[19]. The novelty of this study is the application of an array of lumped-circuit elements to produce a thin two-dimensional structure that must generally be described by band structure concepts, even though the thickness and preiodicity are both much smaller than the operating wavelength.

A. Bumpy Surfaces

Surface waves can be eliminated from a metal surface over a finite frequency band by applying a periodic texture, such as a lattice of small bumps. As surface waves scatter from the rows of bumps, the resulting interference prevents them from propagating, producing a two-dimensional electromagnetic bandgap. Such a structure has been studied at optical frequencies by Barnes *et al.* [8] and Kitson *et al.* [9] using a triangular lattice of bumps, patterned on a silver film.

When the wavelength is much longer than the period of two-dimensional lattice, the surface waves barely notice the small bumps. At shorter wavelengths, the surface waves feel the effects of the surface texture. When one-half wavelength fits between the rows of bumps, this corresponds to the Brillouin zone boundary [10] of the two-dimensional lattice. At this wavelength, a standing wave on the surface can have two possible positions: with the wave crests centered on the bumps, or with the nulls centered on the bumps, as shown in Fig. 3. These two modes have slightly different frequencies, separated by a small bandgap, within which surface waves cannot propagate. Our high-impedance surface can be considered as an extension of this "bumpy surface," in which the bandgap has been lowered in frequency by capacitive loading.

B. Corrugated Surfaces

The high-impedance surface can also be understood by examining a similar structure, the corrugated surface, which

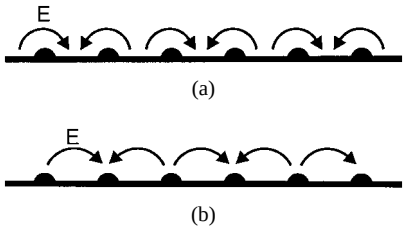

Fig. 3. Bumpy metal sheet has a narrow surface-wave bandgap. (a) Mode at the upper edge of the bandgap, in which the electric field wraps around the bumps. (b) Mode at the lower edge of the bandgap, in which the electric field extends across the bumps.

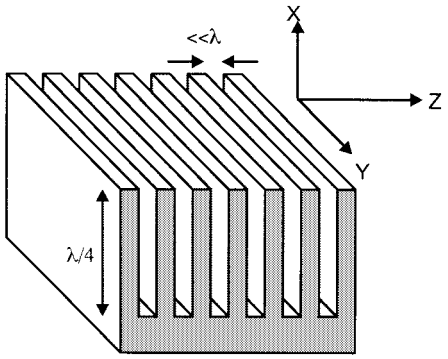

Fig. 4. Corrugated metal slab has high impedance at the top surface if the corrugations are one quarter-wavelength deep.

is discussed in various textbooks [2], [3], and review articles [11], [12]. Numerous authors have also contributed general treatments of corrugated surfaces [13]–[15], and specific studies of important structures [16]–[19]. A corrugated surface is a metal slab, into which a series of vertical slots have been cut, as depicted in Fig. 4. The slots are narrow, so that many of them fit within one wavelength across the slab. Each slot can be regarded as a parallel-plate transmission line, running down into the slab, and shorted at the bottom. If the slots are one quarter-wavelength deep, then the short circuit at the bottom end is transformed by the length of the slots into an open-circuit at the top end. Thus, the impedance at the top surface is very high.

If there are many slots per wavelength, the structure can be assigned an effective surface impedance equal to the impedance of the slots. The behavior of the corrugations is reduced to a single parameter—the boundary condition at the top surface. If the depth of the slots is greater than one quarter-wavelength, the surface impedance is capacitive, and TM surface waves are forbidden. Furthermore, a plane wave polarized with the electric field perpendicular to the ridges will appear to be reflected with no phase reversal since the effective reflection plane is actually at the bottom of the slots, one quarter-wavelength away.

C. High-Impedance Surfaces

The high-impedance surface described here is an abstraction of the corrugated surface, in which the corrugations have been folded up into lumped-circuit elements, and distributed in a two-dimensional lattice. The surface impedance is modeled as a parallel resonant circuit, which can be tuned to exhibit

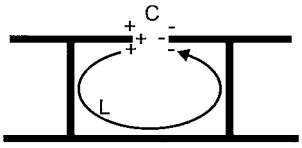

Fig. 5. Origin of the capacitance and inductance in the high-impedance surface.

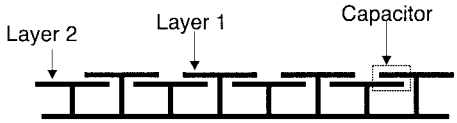

Fig. 6. Three-layer high-impedance surface achieves a lower operating frequency for a given thickness by using capacitive loading, but it also suffers a reduction in bandwidth.

high impedance over a predetermined frequency band. Periodic two- or three-dimensional dielectric [20]–[24], metallic [25]–[28], or metallodielectric [29]–[33] structures that prevent the propagation of electromagnetic waves are known as photonic crystals [34]–[36]. The high-impedance surface can be considered as a kind of two-dimensional photonic crystal that prevents the propagation of radio-frequency surface currents within the bandgap.

As the structure illustrated in Fig. 5 interacts with electromagnetic waves, currents are induced in the top metal plates. A voltage applied parallel to the top surface causes charges to build up on the ends of the plates, which can be described as a capacitance. As the charges slosh back and forth, they flow around a long path through the vias and bottom plate. Associated with these currents is a magnetic field and, thus, an inductance.

We assign to the surface a sheet impedance equal to the impedance of a parallel resonant circuit, consisting of the sheet capacitance and the sheet inductance

$$Z = \frac{j\omega L}{1-\omega^2 LC}. \tag{16}$$

The surface is inductive at low frequencies, and capacitive at high frequencies. The impedance is very high near the resonance frequency ω_0

$$\omega_0 = \frac{1}{\sqrt{LC}}. \tag{17}$$

We associate the high impedance with a forbidden frequency bandgap. In the two-layer geometry shown in Fig. 1, the capacitors are formed by the fringing electric fields between adjacent metal patches, and the inductance is fixed by the thickness of the structure. A three-layer design shown in Fig. 6 achieves a lower resonance frequency for a given thickness by using capacitive loading. In this geometry, parallel-plate capacitors are formed by the top two overlapping layers.

IV. Effective Surface Impedance Model

Some of the properties of the high-impedance surface can be explained using an effective surface impedance model. The surface is assigned an impedance equal to that of a parallel resonant LC circuit, derived by geometry. The use

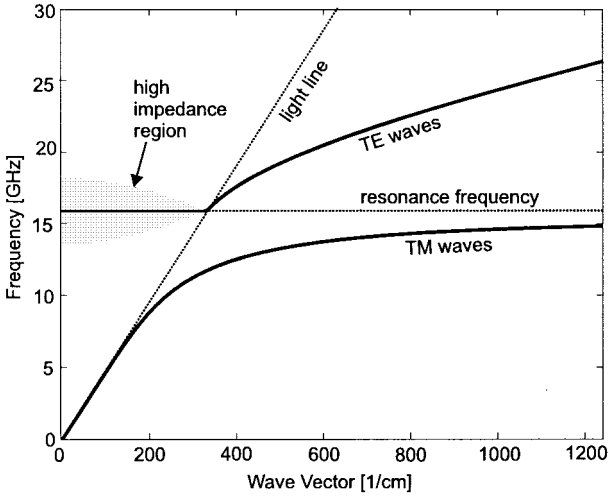

Fig. 7. Dispersion diagram of the high-impedance surface, calculated using the effective surface impedance model.

of lumped parameters to describe electromagnetic structures is valid as long as the wavelength is much longer than the size of the individual features. This short wave vector range is also the regime of effective medium theory. The effective surface impedance model can predict the reflection properties and some features of the surface-wave band structure, but not the bandgap itself, which by definition must extend to large wave vectors.

A. Surface Waves

We can determine the dispersion relation for surface waves in the context of the effective surface impedance model by inserting (1) into Maxwell's equations. The wave vector k is related to the spatial decay constant α and the frequency, ω by the following expression:

$$k^2 = \mu_0\varepsilon_0\omega^2 + \alpha^2. \tag{18}$$

For TM waves we can combine (18) with (14) to find the following expression for k as a function of ω, in which $\eta = \sqrt{\mu_0/\varepsilon_0}$ is the impedance of free space and $c = 1/\sqrt{\mu_0\varepsilon_0}$ is the speed of light in vacuum:

$$k_{\mathrm{TM}} = \frac{\omega}{c}\sqrt{1 - \frac{Z_s^2}{\eta^2}}. \tag{19}$$

We can find a similar expression for TE waves by combining (18) with (15) as follows:

$$k_{\mathrm{TE}} = \frac{\omega}{c}\sqrt{1 - \frac{\eta^2}{Z_s^2}}. \tag{20}$$

By inserting (16) into (19) and (20), we can plot the dispersion diagram for surface waves, in the context of the effective surface impedance model. Depending on geometry, typical values for the sheet capacitance and sheet inductance of a two-layer structure are about 0.05 pF[2], and 2 nH[2], respectively. The complete dispersion diagram, calculated using the effective medium model, is shown in Fig. 7.

Below resonance, TM surface waves are supported. At low frequencies, they lie very near the light line, and the fields extend many wavelengths beyond the surface, as they do on a flat metal surface. Near the resonant frequency, the surface waves are tightly bound to the sheet, and have a very low group velocity, as seen by the fact that the dispersion curve is bent over, away from the light line. In the effective surface impedance limit, there is no Brillouin zone boundary, and the TM dispersion curve approaches the resonance frequency asymptotically. Thus, this approximation fails to predict the bandgap.

Above the resonance frequency, the surface is capacitive, and TE waves are supported. The lower end of the dispersion curve is close to the light line, and the waves are weakly bound to the surface, extending far into the surrounding space. As the frequency is increased, the curve bends away from the light line, and the waves are more tightly bound to the surface. The slope of the dispersion curve indicates that the waves feel an effective index of refraction that is greater than unity. This is because a significant portion of the electric field is concentrated in the capacitors. The effective dielectric constant of a material is enhanced if it is permeated with capacitor-like structures.

The TE waves that lie to the left of the light line exist as leaky waves that are damped by radiation. Radiation occurs from surfaces with a real impedance, thus, the leaky modes to the left-hand side of the light line occur at the resonance frequency. The radiation from these leaky TE modes is modeled as a resistor in parallel with the high-impedance surface, which blurs the resonance frequency. Thus, the leaky waves actually radiate within a finite bandwidth, as shown in Fig. 7. The damping resistance is the impedance of free space, projected onto the surface according to the angle of radiation. Small wave vectors represent radiation perpendicular to the surface, while wave vectors near the light line represent radiation at grazing angles. For a TE polarized plane wave, the magnetic field, H, projected on the surface at angle θ with respect to normal is $H(\theta) = H_0\cos(\theta)$, while the electric field is just $E(\theta) = E_0$. The impedance of free space, as seen by the surface for radiation at an angle, is given by the following expression:

$$Z_{\mathrm{space}}(\theta) = \frac{E(\theta)}{H(\theta)} = \frac{\eta}{\cos(\theta)}. \tag{21}$$

Thus, the radiation resistance is 377 Ω for small wave vectors and normal radiation, but the damping resistance approaches infinity for wave vectors near the light line. Infinite resistance in a parallel resonant circuit corresponds to no damping, so the radiative band is reduced to zero width for grazing angles near the light line. The high-impedance radiative region is shown as a shaded area, representing the blurring of the leaky waves by radiation damping. In place of a bandgap, the effective surface impedance model predicts a frequency band characterized by radiation damping.

B. Reflection Phase

The surface impedance determines the boundary condition at the surface for the standing wave formed by incident and

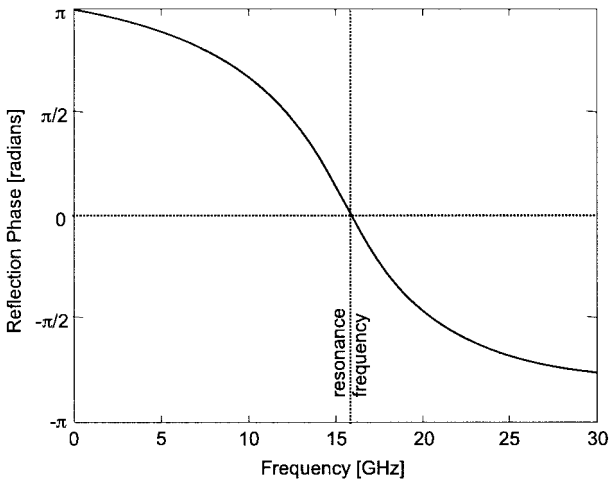

Fig. 8. Reflection phase of the high-impedance surface, calculated using the effective surface impedance model.

reflected waves. If the surface has low impedance, such as in the case of a good conductor, the ratio of electric field to magnetic field is small. The electric field has a node at the surface, and the magnetic field has an antinode. Conversely, for a high impedance surface, the electric field has an antinode at the surface, while the magnetic field has a node. Another term for such a surface is an artificial "magnetic conductor." Recent work involving grounded frequency selective surfaces has also been shown to mimic a magnetic conductor [37]. However, these structures do not possess a complete surface-wave bandgap, since they lack the vertical conducting vias, which interact with the vertical electric field of TM surface waves.

Typical parameters for a two-layer ground plane are 2 nH^2 of inductance, and 0.05 pF^2 of capacitance. For these values, the reflection phase is plotted in Fig. 8. At very low frequencies, the reflection phase is π, and the structure behaves like an ordinary flat metal surface. The reflection phase slopes downward, and eventually crosses through zero at the resonance frequency. Above the resonance frequency, the phase returns to $-\pi$. The phase falls within $\pi/2$ and $-\pi/2$ when the magnitude of the surface impedance exceeds the impedance of free space. Within this range, image currents are in-phase, rather than out-of-phase, and antenna elements may lie directly adjacent to the surface without being shorted out.

C. Radiation Bandwidth

An antenna lying parallel to the textured surface will see the impedance of free space on one side, and the impedance of the ground plane on the other side. Where the textured surface has low impedance, far from the resonance frequency, the antenna current is mirrored by an opposing current in the surface. Since the antenna is shorted out by the nearby conductor, the radiation efficiency is very low. Within the forbidden bandgap near resonance, the textured surface has much higher impedance than free space, so the antenna is not shorted out. In this range of frequencies, the radiation efficiency is high.

Although the surface exhibits high impedance, it is not actually devoid of current. (If there were no current, electromagnetic waves would be transmitted right through the ground plane.) However, the resonant structure provides a phase shift, thus, the image currents in the surface reinforce the currents in the antenna, instead of canceling them.

To the left-hand side of the light line in Fig. 7, we can determine the frequency range over which the radiation efficiency is high by using a circuit model, in which the antenna is modeled as a current source. The textured surface is modeled as an LC circuit in parallel with the antenna, and the radiation into free space is modeled as a resistor with a value of $\sqrt{\mu_0/\varepsilon_0}/\cos(\theta) = 377\ \Omega/\cos(\theta)$. The amount of power dissipated in the resistor is a measure of the radiation efficiency of the antenna.

The maximum power dissipated in the resistor occurs at the LC resonance frequency of the ground plane, where the surface reactance crosses through infinity. At very low frequencies, or at very high frequencies, the current is shunted through the inductor or the capacitor, and the power flowing to the resistor is reduced. It can be shown that the frequencies where the radiation drops to half of its maximum value occur when the magnitude of the surface impedance is equal to the impedance of free space. For normal radiation, we have the following equation:

$$\left|\frac{j\omega L}{1-\omega^2 LC}\right| = \eta. \tag{22}$$

This can be solved for ω to yield the following equation:

$$\omega^2 = \frac{1}{LC} + \frac{1}{2\eta^2 C^2} \pm \frac{1}{\eta C}\sqrt{\frac{1}{LC} + \frac{1}{4\eta^2 C^2}}. \tag{23}$$

For typical geometries, L is usually on the order of 1 nH, and C is in the range of 0.05–10 pF. With these values, the terms involving $1/\eta^2 C^2$ are much smaller than the $1/LC$ terms, so we will eliminate them. This approximation yields the following expression for the edges of the operating band:

$$\omega = \omega_0\sqrt{1 \pm \frac{Z_0}{\eta}}. \tag{24}$$

The resonance frequency is $\omega_0 = 1/\sqrt{LC}$, and $Z_0 = \sqrt{L/C}$ is the characteristic impedance of the LC circuit. With the parameters for L, C, and η given above, Z_0 is usually significantly smaller than η. Thus, the square root can be expanded in the following approximation:

$$\omega \approx \omega_0\left(1 \pm \frac{1}{2}\frac{Z_0}{\eta}\right). \tag{25}$$

The two frequencies designated by the $\pm$ signs delimit the range over which an antenna would radiate efficiently on such a surface. The total bandwidth is roughly equal to the characteristic impedance of the surface divided by the impedance of free space

$$\frac{\Delta\omega}{\omega_0} = \frac{Z_0}{\eta}. \tag{26}$$

This is also the bandwidth over which the reflection coefficient falls between $+\pi/2$ and $-\pi/2$, and image currents are more

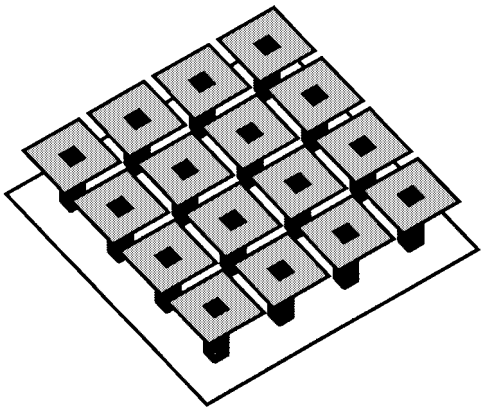

Fig. 9. Square geometry studied using the finite-element model.

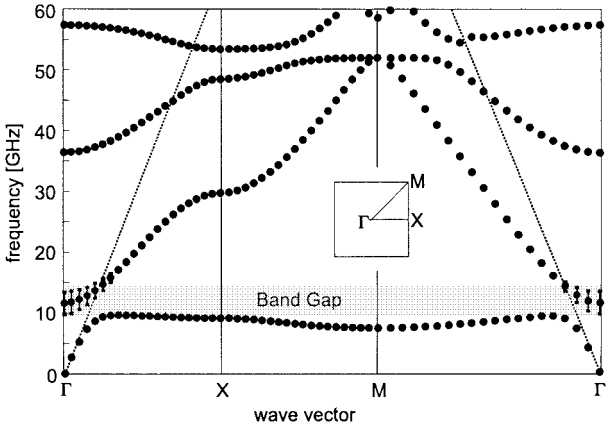

Fig. 10. Surface-wave band structure of the high-impedance surface, calculated using a finite-element model. The radiation broadening of the TE modes above the light line is indicated by error bars.

in-phase than out-of-phase. It represents the maximum usable bandwidth of a flush-mounted antenna on a resonant surface of this type.

The relative bandwidth $\Delta\omega/\omega$ is proportional to $\sqrt{L/C}$, thus, if the capacitance is increased, the bandwidth suffers. Since the thickness is related to the inductance, the more the resonance frequency is reduced for a given thickness, the more the bandwidth is diminished.

V. Finite-Element Model

In the effective surface impedance model described above, the properties of the surface are summarized into a single parameter, namely the surface impedance. Such a model correctly predicts the reflection properties of the high-impedance surface, and some features of the surface-wave bands. However, it does not predict an actual bandgap. Nevertheless, we have found experimentally that the surface-wave bandgap edges occur where the reflection phase is equal to $\pm\pi/2$, thus, this generally corresponds to the width of the surface-wave bandgap. Within this region, surface currents radiate.

It is necessary to obtain more accurate results using a finite-element model, in which the detailed geometry of the surface texture is included explicitly. In the finite-element model, the metal and dielectric regions of one unit cell are discretized on a grid. The electric field at all points on the grid can be reduced to an eigenvalue equation, which may be solved numerically. Bloch boundary conditions are used, in which the fields at one edge of the cell are related to the fields at the opposite edge by the wave vector. The calculation yields the allowed frequencies for a particular wave vector, and the procedure is repeated for each wave vector to produce the dispersion diagram. The structure analyzed by the finite-element method was a two-layer high-impedance surface with square geometry, shown in Fig. 9. The lattice constant was 2.4 mm, the spacing between the plates was 0.15 mm, and the width of the vias was 0.36 mm. The volume below the square plates was filled with $\varepsilon = 2.2$, and the total thickness was 1.6 mm.

The results of the finite-element calculation are shown in Fig. 10. The TM band follows the light line up to a certain frequency, where it suddenly becomes very flat. The TE band begins at a higher frequency, and continues upward with a slope of less than the vacuum speed of light, which is indicated

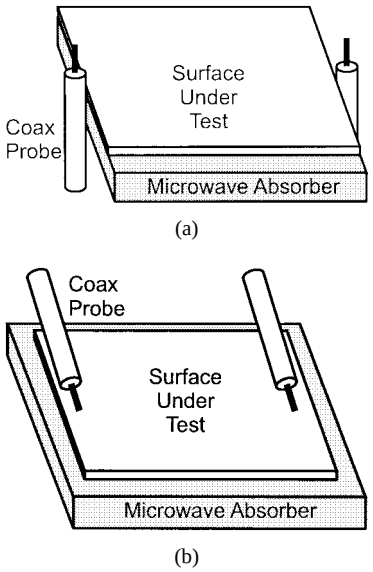

Fig. 11. (a) TM surface-wave measurement using vertical monopole probe antennas. The probes couple to the vertical electric field of TM surface waves. (b) TE surface-wave measurement using horizontal monopole probe antennas. The probes couple to the horizontal electric field of TE surface waves.

on the graph by a dotted line. These results agree qualitatively with the effective medium model. The finite-element method also predicts higher frequency bands that are seen in the measurements, but do not appear in the effective medium model.

According to the finite-element model, the TM band does not reach the TE band edge, but stops below it, forming a bandgap. The TE band slopes upward upon crossing the light line. Thus, the finite-element model predicts a surface-wave bandgap that spans from the edge of the TM band, to the point where the TE band crosses the light line. The resonance frequency is centered in the forbidden bandgap.

In both the TM and TE bands, the $k = 0$ state represents a continuous sheet of current. The lowest TM mode, at zero frequency, is simply a sheet of constant current—a dc mode. The highest TM mode, at the Brillouin zone edge, is a standing wave in which each row of metal protrusions has opposite

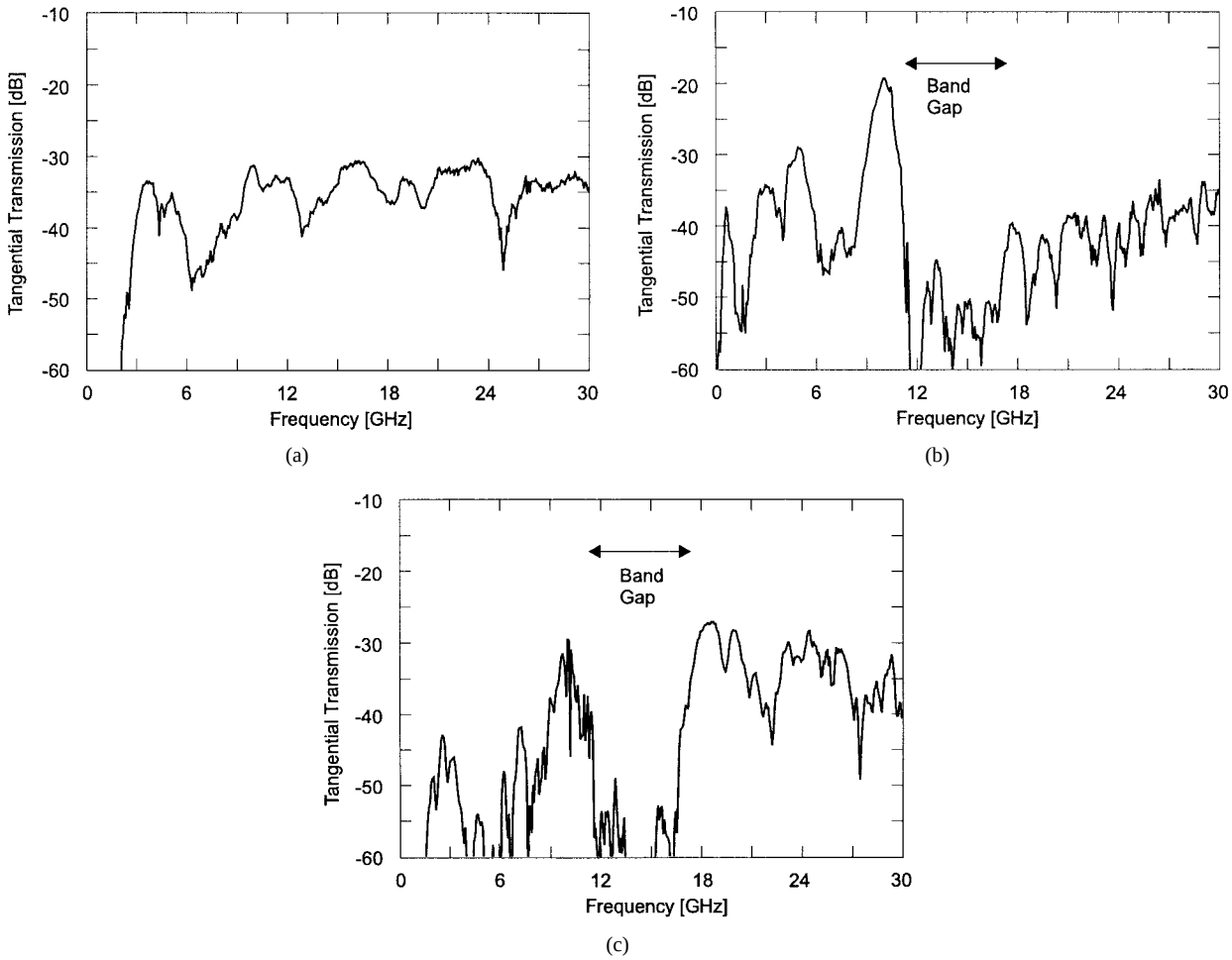

Fig. 12. (a) TM surface-wave transmission across a flat metal surface. (b) TM surface-wave transmission across a two-layer high-impedance surface. (c) TE surface-wave transmission across a two-layer high-impedance surface. The strong fluctuations are due to multipath interference. The forbidden bandgap is shown for cases (b) and (c).

charge. The lowest TE mode is a sheet of current that is continuous in space, but oscillating at the LC resonance frequency, at the origin of k-space. The TE band slopes smoothly upward in frequency, crossing through the light line at some point. At the highest TE mode, at the Brillouin zone boundary, transverse currents flow in opposite directions on each row of protrusions.

In the other upper bands, the electric field is primarily concentrated in the region below the capacitor plates. The modes in these bands resemble the modes in a parallel-plate waveguide. The first of these modes occurs at about the frequency where one half-wavelength fits between the rows of metal vias.

VI. Measuring Surface Properties

A. Surface Waves

Since surface waves cannot generally couple to external plane waves, specialized methods must be used to measure them. At optical frequencies, surface plasmons are often studied using a technique called prism coupling [8]. A prism is placed next to the surface, and the refractive index of the prism is used to match the wave vector of a probe beam to that of a surface wave. Another method for coupling to surface waves, which is more practical at microwave frequencies, is to use a very small probe. A point source launches all wave vectors, thus, a small antenna brought near the surface is capable of coupling to surface-wave modes. The antenna geometry can be tailored to distinguish surface-wave polarization.

In TM surface waves, the electric field forms loops that extend vertically out of the surface. TM waves can be measured using a pair of small monopole antennas oriented normally with respect to the surface, as shown in Fig. 11(a). The vertical electric field of the probe couples to the vertical electric field of the TM surface waves. In TE surface waves, the electric field is parallel to the surface. They can be measured with a pair of small monopole probes oriented parallel to the sheet, as shown in Fig. 11(b). The horizontal electric field of the antenna couples to the horizontal electric field of the TE waves.

On a flat metal sheet, a TM surface-wave measurement produces the results shown in Fig. 12(a). The surface under test was a 12-cm^2 sheet of flat metal. The measurement represents the transmission between a pair of monopole probes oriented vertically at the edges of the metal sheet. (A TE surface-wave measurement produces no significant signal because any antenna that excites TE waves is shorted out on a conducting

surface. It is only on the textured surface, with its unusual surface impedance, that significant TE transmission signal levels can be obtained.)

The TM data has variations of 10–15 dB, but remains relatively flat over a broad spectrum. The variations are produced by multipath interference, or speckle, which occurs in coherent measurements whenever multiple signal paths are present. Multipath interference can be distinguished from other effects because it is characterized by narrow-band fading, whose details depend on the exact antenna position. The transmission drops off at low frequencies because the small probes are inefficient at exciting long wavelengths.

A typical TM surface-wave measurement on a textured surface is shown in Fig. 12(b). The size of the sheet and the measurement technique were the same as those used for the flat metal surface. The structure consisted of a triangular array of hexagonal patches as shown in Fig. 1, with a period of 2.54 mm and a gap between the patches of 0.15 mm. The thickness of the board was 1.55 mm, and the dielectric constant was 2.2.

The transmission is strong at low frequencies, and exhibits the same multipath interference seen on the metal surface. At 11 GHz, the transmission drops by about 30 dB, indicating the edge of the TM surface-wave band. Beyond this frequency, the transmission level remains low and flat, eventually sloping upward at much higher frequencies because of weak coupling to TE surface waves. The TE band edge is not apparent in this measurement, but the region corresponding to the surface-wave bandgap is indicated on the graph by an arrow.

A TE transmission measurement of the same textured surface is shown in Fig. 12(c). It was taken using a pair of small coaxial probes, oriented parallel to the surface. The transmission is weak at low frequencies, and strong at high frequencies, the reverse profile of the TM data. A sharp jump of 30 dB occurs at 17 GHz, indicating the TE band edge. Beyond this frequency, the transmission is flat, with only small fluctuations due to speckle. The TE probes also couple slightly to TM surface waves, so there is an additional transmission peak at 11 GHZ, at the TM band edge, where the density of TM states is high. Both TM and TE probes tend to couple slightly to the opposite surface-wave polarizations. However, the cross coupling is greater with the TE probe because it lacks the symmetry of the vertical monopole.

A surface-wave bandgap is measured between the TM band edge at 11 GHz and the TE band edge at 17 GHz. Within this range, neither polarization produces significant transmission. Currents cannot propagate across the surface, and any induced currents radiate from the surface.

B. Reflection Phase

The reflection phase of the high-impedance surface can be measured using two microwave horn antennas, as shown in Fig. 13. The measurement is done in an anechoic chamber lined with microwave absorbing foam. The two horns are placed next to each other, aimed at the surface. Two windows are cut in the chamber, one for the antennas, and one for the surface under test.

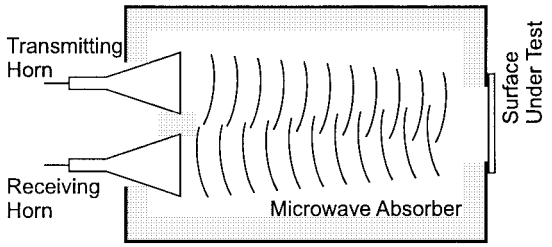

Fig. 13. Reflection phase measurement performed using a pair of horn antennas. The anechoic chamber used in these experiments measured 30 cm × 30 cm × 60 cm, and the hole for the sample measured 10 cm × 10 cm.

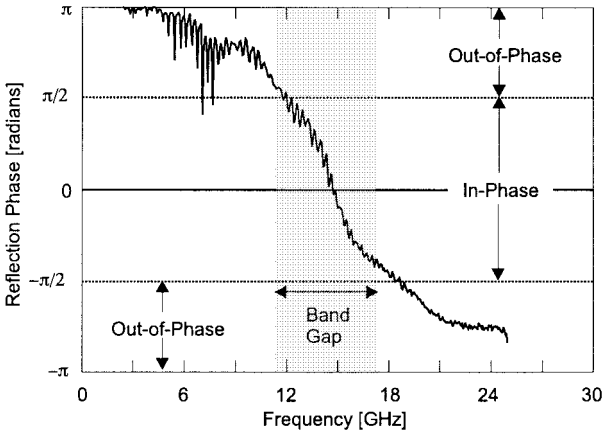

Fig. 14. Measured reflection phase of a two-layer high-impedance surface.

A reference measurement is taken of a surface with known reflection properties, such as a flat sheet of metal, and all subsequent measurements are divided by this reference. A factor of π is added to the phase data to account for the reference scan of the metal sheet, which is known to have a reflection phase of π.

The reflection phase of the high impedance surface is shown in Fig. 14. At low frequencies, it reflects with a π phase shift just like a metal surface. As the frequency is increased, the phase slopes downward, and eventually crosses through zero at the resonance frequency of the structure. At higher frequencies, the phase continues to slope downward, and eventually approaches $-\pi$. Within the region between $\pi/2$ and $-\pi/2$, indicated on the graph by arrows, plane waves are reflected in-phase, rather than out-of-phase. This range also corresponds to the measured surface-wave bandgap, indicated on the graph by a shaded region, with the TM and TE band edges falling approximately at the points where the phase crosses through $\pi/2$ and $-\pi/2$, respectively.

C. Low-Frequency Structures

With two-layer construction, the capacitors are formed by the fringing capacitance between two metal plates lying edge-to-edge, usually separated by a few hundred microns. If the substrate has a dielectric constant between 2–10, and the period is a few millimeters, the capacitance is generally on the order of a few tens of femtofarads. With a thickness of a few millimeters, the inductance is a few nanohenrys, so the resonance frequency is on typically the order of about 10 GHz.

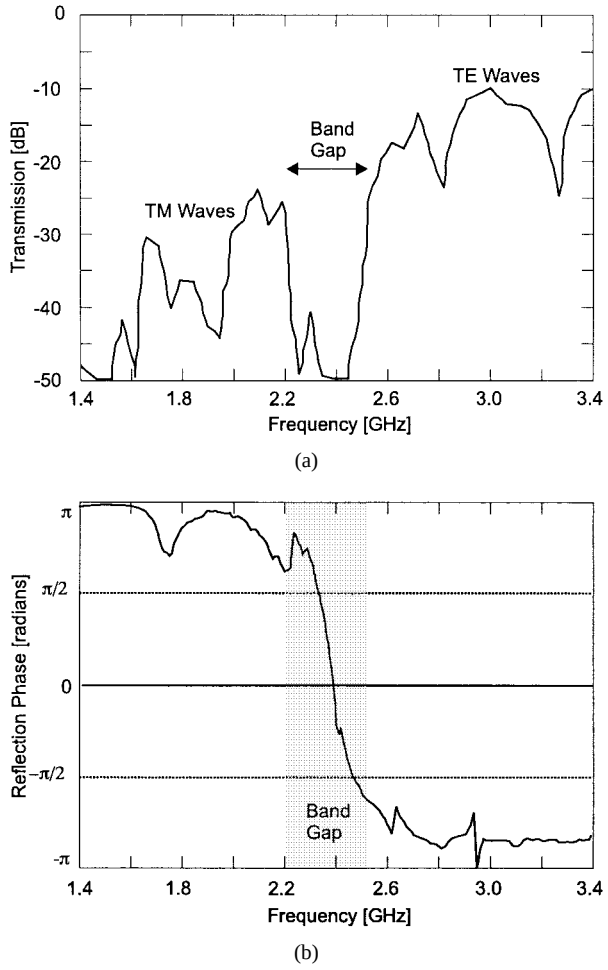

Fig. 15. (a) Surface-wave transmission across a three-layer high-impedance surface. The lower resonance frequency is achieved through capacitive loading. (b) Reflection phase of a three-layer high-impedance surface.

If the desired resonance frequency is less than about 5 GHz, the thickness can be kept within reasonable limits by using three-layer construction, in which the capacitors are formed between overlapping metal plates, as in Fig. 6. With this method, a capacitance of several picofarads is easily achievable. Resonance frequencies of less than 1 GHz can be produced, while maintaining the thickness and period on the order of a few millimeters. However, by forcing a thin structure to have a low resonance frequency, the bandwidth is also reduced.

The three-layer high-impedance surface maintains the same general properties as the two-layer structure, with TM and TE surface-wave bands separated by a gap, within which there are no propagating surface-wave modes. A surface-wave measurement is shown in Fig. 15(a) for a typical three-layer structure. This sample had a hexagonal lattice with a period of 6.35 mm, and an overlap area between adjacent metal plates of 6.84 mm^2. The spacer layer between the plates had a thickness of 100 μm, and a dielectric constant of 3.25. The thickness of the lower supporting board was 3.17 mm, with a dielectric constant of 4.0. The data shows the transmission between two straight coaxial probes lying parallel to the surface, in what is usually considered the TE configuration. The frequency is

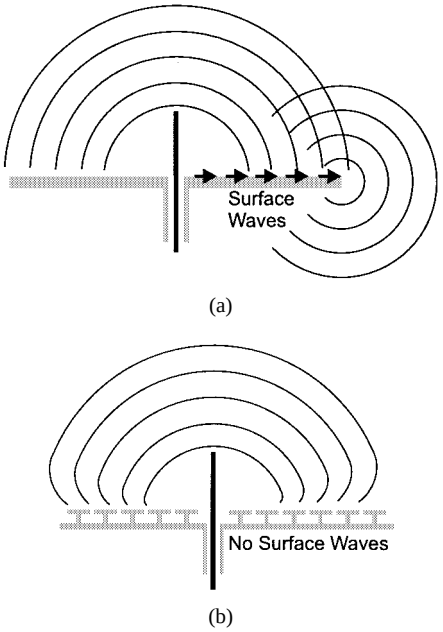

Fig. 16. (a) Antenna on a flat metal ground plane generates propagating surface currents, which cause multipath interference and backward radiation. (b) Surface waves are suppressed on a high-impedance ground plane.

low enough that the free-space wavelength is much greater than the probe length, which is only a few millimeters, so the antennas tend to couple equally well to TM and TE modes. Transmission can be seen in both the TM and TE bands, and a gap is visible between 2.2–2.5 GHz.

The reflection phase is shown in Fig. 15(b). The region corresponding to the surface-wave bandgap is shaded. Inside this gap, the reflection phase crosses through zero, and plane waves are reflected in-phase rather than out-of-phase.

VII. Antennas

The high-impedance surface has proven useful as an antenna ground plane. Related research has also been done on conventional three-dimensional photonic crystals [38]–[42], but those depend on different principles. Using high-impedance ground planes, antennas have been demonstrated that take advantage of both the suppression of surface waves, and the unusual reflection phase. An antenna on a high-impedance ground plane produces a smoother radiation profile than a similar antenna on a conventional metal ground plane, with less power wasted in the backward direction. Furthermore, radiating elements can lie directly adjacent to the high-impedance surface without being shorted out. These antennas can take on a variety of forms, including straight wires to produce linear polarization, or various other shapes to generate circular polarization. Patch antennas are also improved if they are embedded in a high-impedance surface.

The high-impedance surface is particularly applicable to the field of portable hand-held communications, in which the interaction between the antenna and the user can have a significant impact on antenna performance. Using this new ground plane as a shield between the antenna and the user in portable communications equipment can lead to higher antenna efficiency, longer battery life, and lower weight.

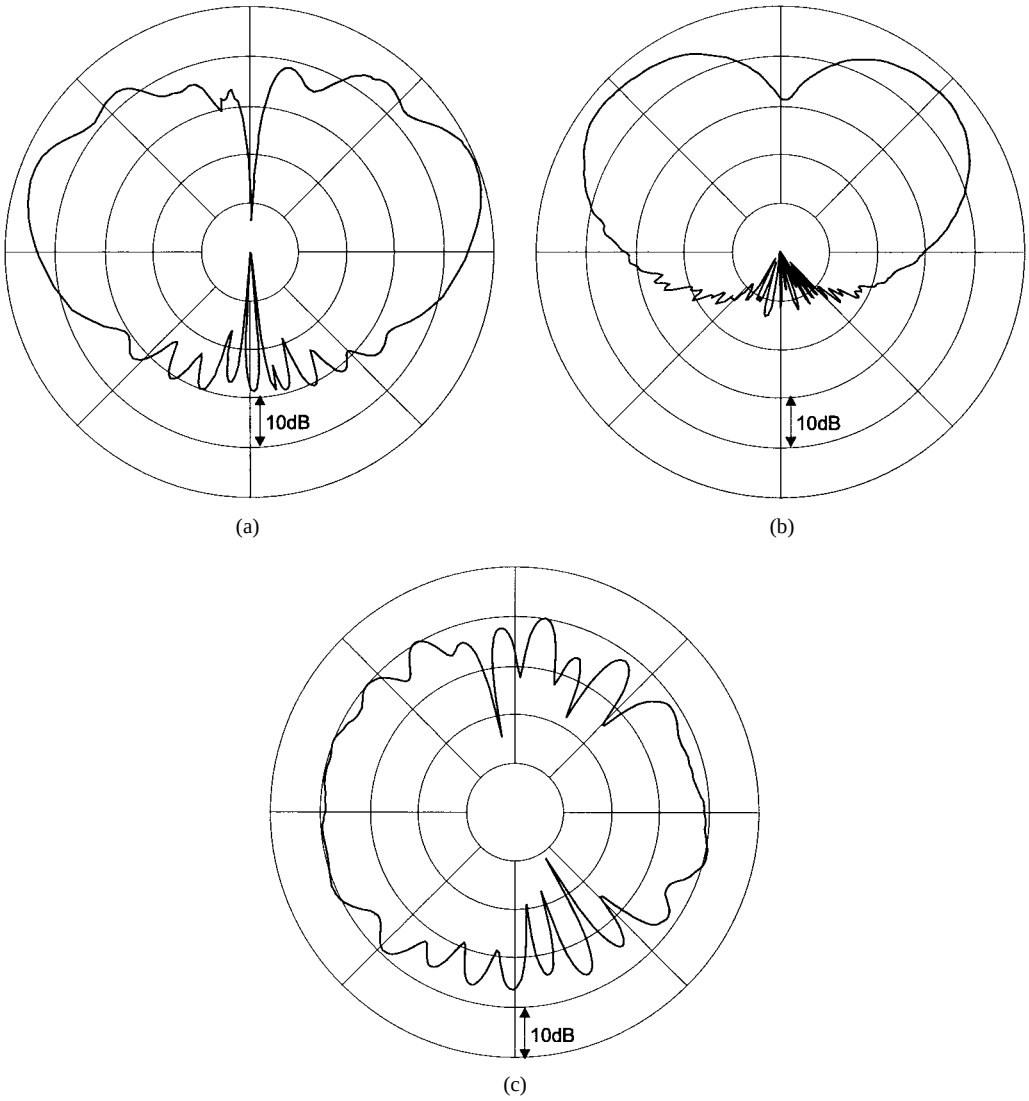

Fig. 17. (a) Radiation pattern of a monopole antenna on a flat metal ground plane contains many lobes and nulls due to multipath interference from surface waves. (b) Radiation pattern of a monopole on a high-impedance ground plane is smooth, due to the suppression of surface waves. (c) Within the allowed TM surface-wave band, the high-impedance ground plane behaves as an ordinary flat metal ground plane, similar to (a).

A. The Vertical Monopole

One of the simplest antennas is a vertical monopole, shown in Fig. 16(a). It can be fabricated by feeding a coaxial cable through a metal sheet, and extending the center conductor to form a radiating wire. The outer conductor is shorted to the metal surface, which acts as a ground plane.

On an infinitely large ground plane, an antenna of this type would ideally have a smooth half-doughnut-shaped radiation pattern, with a null on the axis of the wire, and no radiation in the backward direction. In reality, the ground plane is always finite, and its edges contribute to the radiation pattern. In addition to space waves, the antenna generates surface waves in the ground plane, which then radiate from edges and corners. The combined radiation from the wire and the ground plane edges interfere to form a series of multipath lobes and nulls at various angles, as shown in Fig. 17(a). The edges also radiate backward, causing a significant amount of wasted power in the backward hemisphere.

If the metal ground plane is replaced with a high-impedance ground plane, as shown in Fig. 16(b), the surface waves are suppressed. While driven currents can exist on any reflective surface, they do not propagate on our high-impedance ground plane. Any induced currents are restricted to a localized region around the antenna, and never reach the edges of the ground plane. The absence of multipath interference results in a smoother radiation pattern, with less wasted power in the backward hemisphere, as shown in Fig. 17(b).

For the radiation pattern in Fig. 17(a), the antenna was 3-mm long, and the ground plane was 5 cm^2. The frequency of the measurement was 35 GHz. The important features are the ripples that appear in the forward direction, and the amount of wasted power in the backward direction. These effects are both due to surface waves that propagate away from the antenna and radiate from the ground plane edges.

For the radiation pattern in Fig. 17(b), the flat metal ground plane is replaced with a textured two-layer high-impedance ground plane, with a thickness of 1 mm and a triangular lattice with a period of 1.4 mm. The TM band edge of this surface was at 30 GHz, and the measurement was performed at 35 GHz, within the surface-wave bandgap. The radiation pattern in the

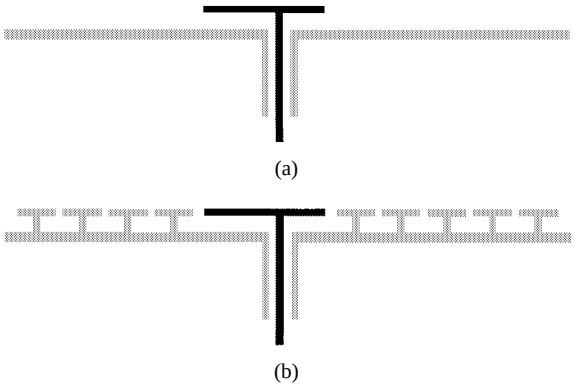

Fig. 18. (a) Patch antenna on a metal ground plane. (b) Patch antenna embedded in a high-impedance ground plane.

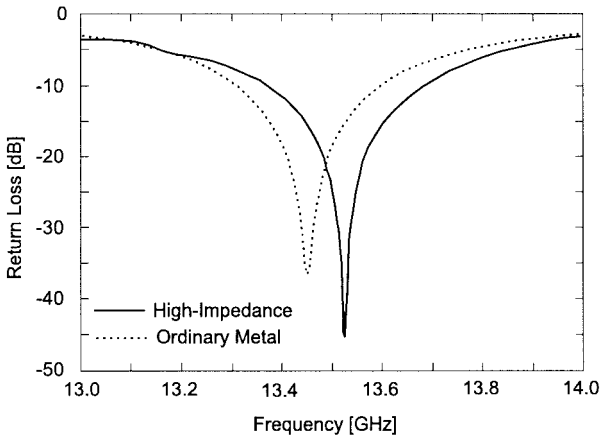

Fig. 19. Measured return loss for patch antennas on two different ground planes.

forward direction is smooth, showing only the two main lobes, and the power wasted in the backward direction is significantly reduced.

Two additional features are apparent in Fig. 17(b). First, the center null is diminished because of asymmetry in the local geometry of the antenna wire and the surrounding metal patches. With more symmetrical construction, the null could be recovered. Second, the received power is lower with the high-impedance ground plane, especially at the horizon. This is because the image currents on the high-impedance ground plane are reversed with respect to their direction on a metal ground plane. For a vertical monopole, this tends to cancel the antenna current, particularly at the horizon.

If the antenna is operated outside the bandgap, the ground plane behaves very much like an ordinary flat sheet of metal. Fig. 17(c) shows the radiation pattern of the monopole antenna on the high-impedance ground plane, operated within the TM surface-wave band, at a frequency of 26 GHz. Due to the presence of surface waves, the pattern contains many lobes and nulls, and a significant amount of power is wasted in the backward hemisphere.

B. The Patch Antenna

The beneficial effects of surface-wave suppression can also be applied to patch antennas. An example of a patch antenna fed using a coaxial probe is shown in Fig. 18(a). The radiation pattern of the patch antenna is degraded by surface waves in much the same way as the wire monopole. Surface waves radiate from the edges of the ground plane, causing ripples in the antenna pattern, and radiation in the backward direction. If the substrate is thick, or it has a high dielectric constant, the surface-wave problem is exacerbated.

Surface waves can be suppressed by embedding the patch in a high-impedance ground plane, as shown in Fig. 18(b). The presence of the nearby metal protrusions tends to raise the resonance frequency of the patch because the effective cavity volume is reduced. This can be corrected by leaving a small guard ring of bare substrate around the patch, or by adjusting the size of the patch.

Fig. 19 shows the return loss at the coax feed of two patch antennas—one on an ordinary metal ground plane, and one on a high-impedance ground plane. In both cases shown, the substrate has a dielectric constant of 10.2, a thickness of 0.625 mm, and a size of 5 cm^2. Circular patches were used, with a diameter of 3.5 mm. The patch on the high-impedance ground plane was separated from the metal protrusions of the surrounding high-impedance surface by a guard ring consisting of 3 mm of bare dielectric. The high-impedance surface used for this antenna was a two-layer structure with a triangular lattice, a period of 2 mm, and a bandgap spanning roughly 12–16 GHz.

The radiation patterns of the two antennas are shown in Fig. 20. The measurements are at a frequency of 13.5 GHz, where the two antennas have the same return loss. In both the H- and E-planes, the patch on the ordinary metal ground plane shows significant radiation in the backward direction, and ripples in the forward direction. Furthermore, the pattern is not rotationally symmetric, and is much thinner in the H-plane than in the E-plane. Conversely, the patch on the high-impedance ground plane produces a smooth symmetric pattern with little backward radiation.

C. The Horizontal Wire Antenna

The benefits of surface-wave suppression have been established through two examples: the vertical monopole and the patch antenna. The other important property of the high-impedance surface is that its image currents are in-phase rather than out-of-phase. This unusual property allows antennas to be constructed that are not possible on a flat conducting ground plane. An example, shown in Fig. 21(a), is a wire antenna that has been bent over so that it lies parallel to the ground plane. A horizontal wire radiates very poorly on an ordinary metal ground plane because the image currents cancel the currents in the antenna. A similar wire antenna on a high-impedance ground plane is shown in Fig. 21(b). This antenna performs well because the image currents in the high-impedance ground plane reinforce the currents in the antenna.

The return loss of the horizontal antenna on the metal ground plane is shown in Fig. 22. Most of the power is reflected back toward the generator, thus, the radiation efficiency is poor. In this example, the antenna was 1-cm long, and separated by a distance of 1 mm from a 3-cm^2 ground plane.

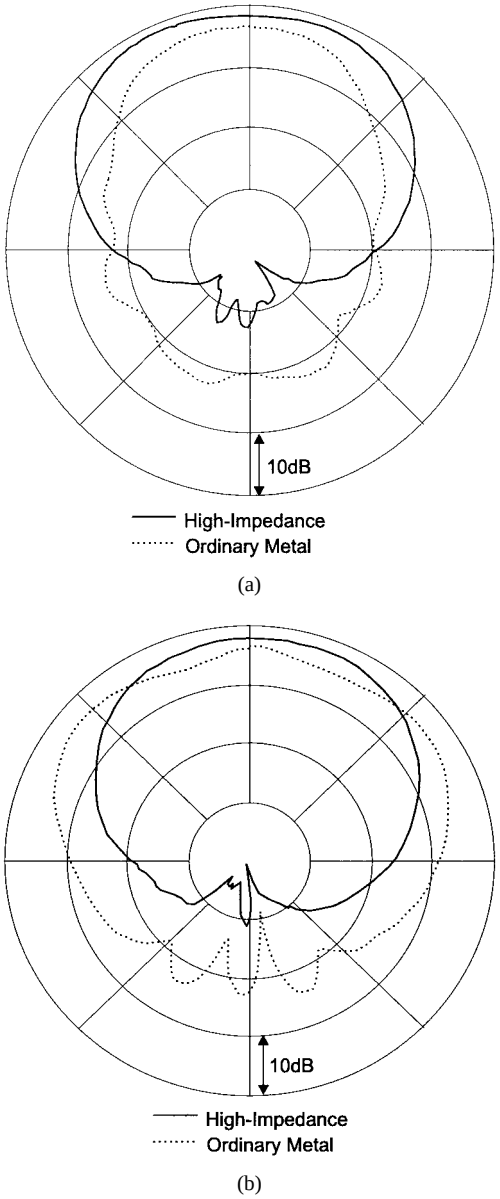

Fig. 20. (a) H- and (b) E-plane radiation patterns of patch antennas on two different ground planes.

The return loss of the antenna is much lower (-10 dB) on the high-impedance ground plane, also shown in Fig. 22. In this measurement, the high-impedance ground plane was identical to the one measured in Figs. 12 and 14, with a bandgap spanning from 11 to 17 GHz. Below the TM band edge, the antenna performance is poor, and similar to the metal ground plane. The surface impedance is low, and the image currents cancel the antenna currents. Within the bandgap, with a return loss of -10 dB, only 10% of the power is being reflected back to the generator. In this range, the image currents are reversed, and they reinforce the antenna currents.

Above the TE band edge, the return loss is low because of coupling to TE surface waves. There is also strong coupling to TM waves near the TM band edge, below the bandgap where the density of states is very high. In both cases, the low return loss is not accompanied by good antenna radiation. Although the antenna radiates over a broad band, it is only useful within

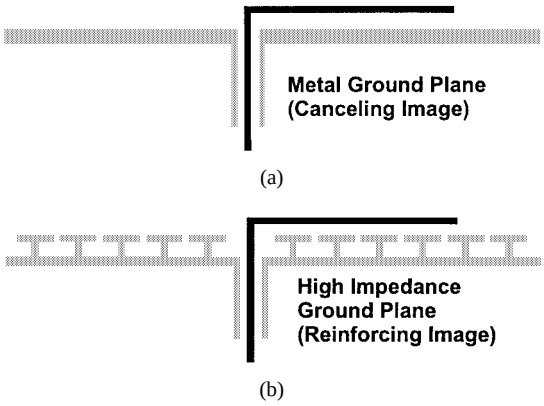

Fig. 21. (a) Horizontal wire antenna on a metal ground plane. Image currents interfere destructively. (b) Horizontal wire antenna on a high-impedance ground plane. Image currents interfere constructively.

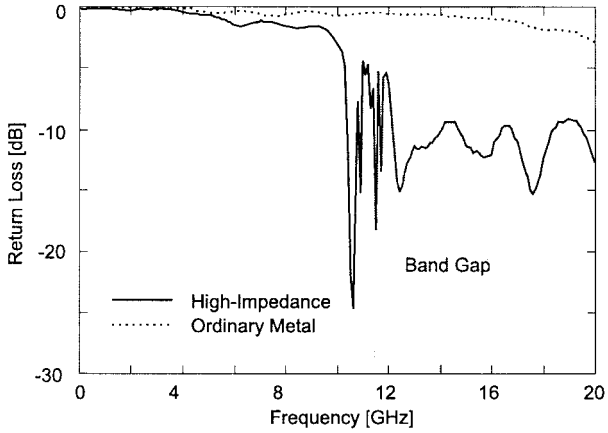

Fig. 22. Return loss in the coax feed of a horizontal wire antenna on two different ground planes.

the surface-wave bandgap, where it produces a smooth pattern. Outside the bandgap, the pattern contains many lobes and nulls due to excitation of propagating surface waves. The radiation pattern for the metal ground plane and the high-impedance ground plane is shown in Fig. 23. The data in the radiation patterns supports the return loss data, in that the signal level is about 10 dB higher on the high-impedance ground plane.

D. Portable Communications

One important application of the high-impedance ground plane is in the area of portable communications. At present, the standard antenna geometry is a monopole, which is part of the handset and lies in close proximity to the user's head. It has been shown that with this configuration, roughly 50% of the radiated power is absorbed by the user [43]. The effect of the radiation on the user has not been evaluated conclusively, but the effect of the user on the antenna is significant. If this lost power could be reclaimed, the benefits for portable communication equipment could be an improvement in battery life, or a reduction in battery weight.

The power lost to absorption can be reduced by using a directional antenna. Directional antennas might appear impractical for portable communications. However, in a real environment, scattering from buildings and other objects tends

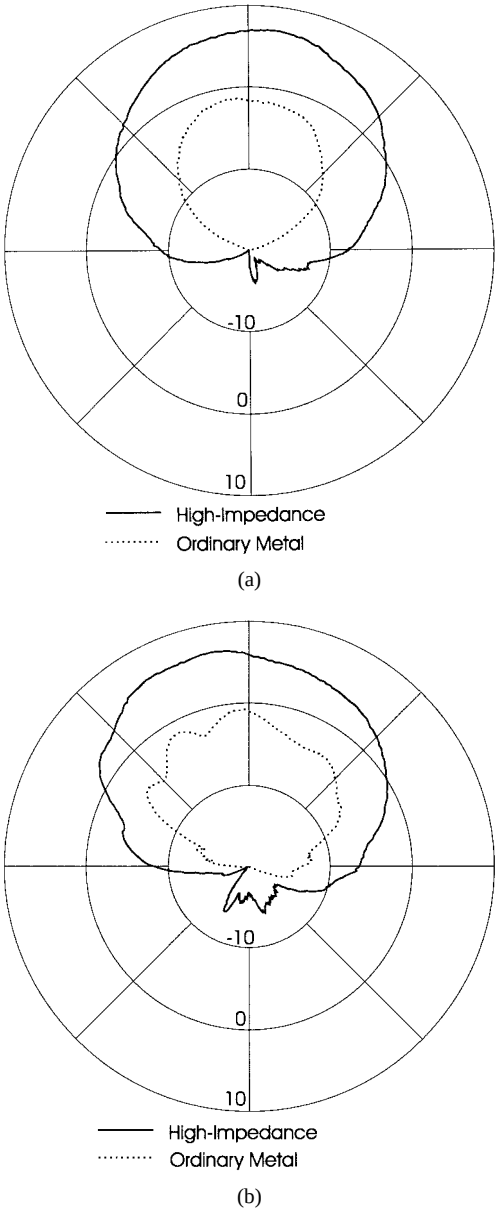

Fig. 23. (a) E- and (b) H-plane radiation pattern of two horizontal wire antennas, measured at a frequency of 13 GHz.

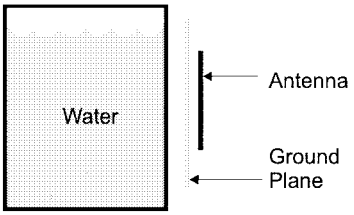

Fig. 24. Experiment to measure effects of the user in portable communications, modeling the user's head as a jar of water.

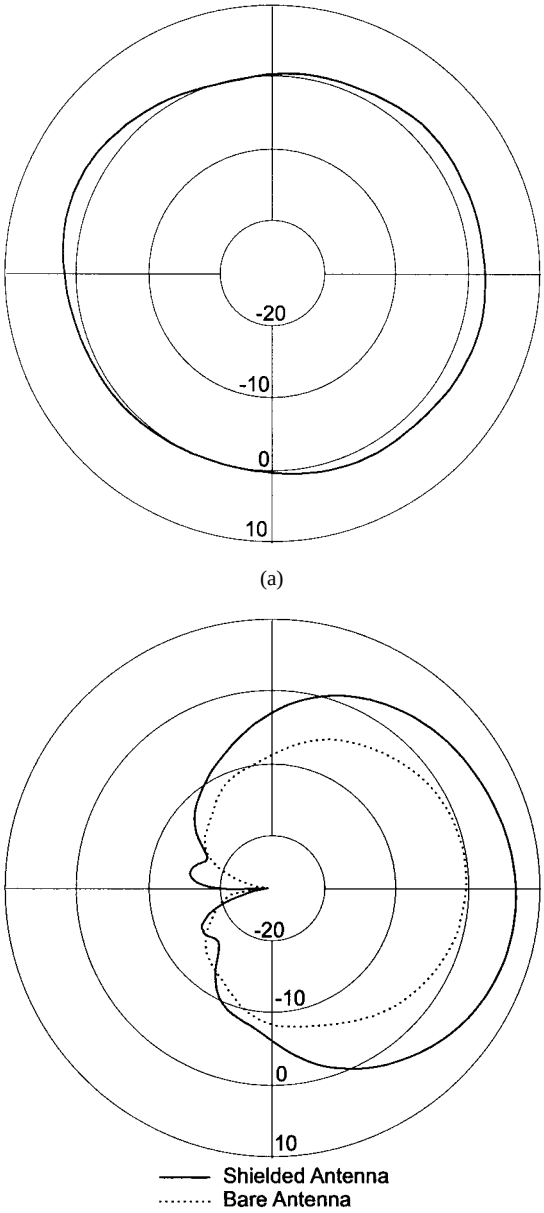

Fig. 25. (a) Reference radiation pattern of a dipole antenna in free space. (b) Radiation pattern of a dipole antenna near the jar of water, and a dipole shielded from the water by a high-impedance ground plane. The antenna efficiency of the shielded antenna is about 90%±10%, comparable to the free space case.

to randomize the signal direction. For commercial products, cost is the most significant design factor, thus, the antenna must be inexpensive to produce, and simple to integrate into the handset hardware. Patch antennas are cheap, but they have the disadvantage that they are easily detuned by nearby dielectric objects. Wire antennas are not as easily detuned, but they are only directional when combined with a reflector. If the reflector is a flat metal sheet, it requires a minimum thickness of one quarter-wavelength, which is impractical. A good alternative is a high-impedance ground plane, with a horizontal wire antenna mounted directly adjacent to the top surface. The frequency of operation is determined by the surface rather than the wire, and since the surface resonance is controlled by the internal coupling between the individual elements, the structure is not readily detuned.

The experiment shown in Fig. 24 is designed to simulate a real communications environment. The presence of the user is modeled by a jar of tap water measuring roughly 15-cm diameter by 20 cm tall. The dielectric constant of water is

similar to most human tissues. Fig. 25(a) shows the H-plane radiation pattern of a half-wave dipole antenna in free space, to be used as a reference. The frequency of the measurement is 2.3 GHz. The radial scale is decibels with respect to an isotropic radiator (dBi), and the dipole has the expected average gain value of around 2 dBi.

The plot shown in Fig. 25(b) is the H-plane radiation pattern of the same dipole antenna placed near the jar of water, oriented in the direction of the jar axis. The radiation is blocked from propagating through the water, as indicated by the deep null in the direction of the jar. The overall signal level is also reduced in all directions due to a combination of absorption and modification of the antenna input impedance. The maximum gain is about 0 dBi, in the direction away from the jar of water.

The radiation pattern shown in Fig. 25(c) was produced by a wire antenna on a high-impedance ground plane. The surface wave and reflection properties of the ground plane used here are shown in Fig. 15. The jar of water was placed behind the ground plane, on the opposite side from the antenna, and the antenna was oriented in the direction of the jar axis. The antenna has a maximum gain of about 6 dBi in the direction normal to the ground plane. The high-impedance surface acts as a shield between the radiating antenna and the absorbing water, blocking not only the direct radiation, but also the surface currents that would wrap around to the back side. The ground plane redirects the radiation that would otherwise be absorbed into the user, recovering it as useful power in the opposite direction. The combination of the antenna and the ground plane is compact and lightweight, allowing it to fit within the packaging of most portable communications equipment.

VIII. Conclusion

A new type of metallic electromagnetic structure has been developed that is characterized by having high surface impedance. It is made of continuous metal, and conducts dc currents, but it does not conduct ac currents within a forbidden frequency bandgap. Instead, any currents that are induced in the surface radiate efficiently into surrounding space. This new surface also reflects electromagnetic waves with no phase reversal, behaving as a kind of artificial magnetic conductor. The structure can be described using a lumped parameter circuit model, which predicts some of its electromagnetic properties. This unique material is applicable to a variety of electromagnetic problems, including new kinds of low-profile antennas.

References

[1] C. Balanis, *Antenna Theory, Analysis, and Design*, 2nd ed. New York: Wiley, 1997.

[2] S. Ramo, J. Whinnery, and T. Van Duzer, *Fields and Waves in Communication Electronics*, 2nd ed. New York: Wiley, 1984.

[3] R. Collin, *Field Theory of Guided Waves*, 2nd ed. New York: IEEE Press, 1991.

[4] H. Raether, *Surface Plasmons on Smooth and Rough Surfaces and on Gratings*. Berlin, Germany, Springer-Verlag, 1988.

[5] D. Sievenpiper, "High-impedance electromagnetic surfaces," Ph.D. dissertation, Dept. Elect. Eng., Univ. California at Los Angeles, Los Angeles, CA, 1999.

[6] D. Sievenpiper and E. Yablonovitch, "Circuit and method for eliminating surface currents on metals," U.S. Patent 60/079953, Mar. 30, 1998.

[7] N. Ashcroft and N. Mermin, *Solid State Physics*. Orlando, FL: Saunders College, 1976.

[8] W. Barnes, T. Priest, S. Kitson, and J. Sambles, "Physical origin of photonic energy gaps in the propagation of surface plasmas on gratings," *Phys. Rev. B. Condens. Matter*, vol. 54, pp. 6227–6244, 1996.

[9] S. Kitson, W. Barnes, and J. Sambles, "Full photonic band gap for surface modes in the visible," *Phys. Rev. Lett.*, vol. 77, pp. 2670–2673, 1996.

[10] L. Brillouin, *Wave Propagation in Periodic Structures; Electric Filters and Crystal Lattices*, 2nd ed. New York: Dover, 1953.

[11] A. Harvey, "Periodic and guiding structures at microwave frequencies," *IRE Trans. Microwave Theory Tech.*, vol. 8, pp. 30–61, June 1959.

[12] C. Elachi, "Waves in active and passive periodic structures: A review," *Proc. IEEE*, vol. 64, p. 1666–1698, Dec. 1976.

[13] L. Brillouin, "Wave guides for slow waves," *J. App. Phys.*, vol. 19, pp. 1023–1041, 1948.

[14] W. Rotman, "A study of single-surface corrugated guides," *Proc. IRE*, vol. 39, pp. 952–959, Aug. 1951.

[15] R. Elliot, "On the theory of corrugated plane surfaces," *IRE Trans. Antennas Propagat.*, vol. 2, pp. 71–81, Apr. 1954.

[16] S. Lee and W. Jones, "Surface waves on two-dimensional corrugated surfaces," *Radio Sci.*, vol. 6, pp. 811–818, 1971.

[17] Y.-L. Chen and Y. Lo, "Reactive reflectors," *Proc. Inst. Elect. Eng.*, pt. H, vol. 131, pp. 263–269, 1984.

[18] P.-S. Kildal, "Artificially soft and hard surfaces in electromagnetics," *IEEE Trans. Antennas Propagat.*, vol. 38, pp. 1537–1544, Oct. 1990.

[19] Z. Ying, P.-S. Kildal, and A. Kishk, "Study of different realizations and calculation models for soft surfaces by using a vertical monopole on a soft disk as a test bed," *IEEE Trans. Antennas Propagat.*, vol. 44, pp. 1474–1481, Nov. 1996.

[20] E. Yablonovitch, "Inhibited spontaneous emission in solid-state physics and electronics," *Phys. Rev. Lett.*, vol. 58, pp. 2059–2062, 1987.

[21] K.-M. Ho, C. Chan, and C. Soukoulis, "Existence of a photonic gap in periodic dielectric structures," *Phys. Rev. Lett.*, vol. 65, pp. 3152–3155, 1990.

[22] C. Chan, K.-M. Ho, and C. Soukoulis, "Photonic band gaps in experimentally realizable periodic dielectric structures," *Europhys. Lett.*, vol. 16, pp. 563–566, 1991.

[23] S. Fan, P. Villeneuve, R. Meade, and J. Joannopoulos, "Design of three-dimensional photonic crystals at submicron lengthscales," *Appl. Phys. Lett.*, vol. 65, p. 1466–1469, 1994.

[24] E. Ozbay, A. Abeyta, G. Tuttle, M. Tringides, R. Biswas, C. Chan, C. Soukoulis, and K.-M. Ho, "Measurement of a three-dimensional photonic band gap in a crystal structure made of dielectric rods," *Phys. Rev. B, Condens. Matter*, vol. 50, pp. 1945–1951, 1994.

[25] D. Smith, S. Schultz, N. Kroll, M. Sigalas, K.-M. Ho, and C. Soukoulis, "Experimental and theoretical results for a two-dimensional metal photonic band-gap cavity," *Appl. Phys. Lett.*, vol. 65, pp. 645–648, 1994.

[26] M. Sigalas, C. Chan, K.-M. Ho, and C. Soukoulis, "Metallic photonic band-gap materials," *Phys. Rev. B, Condens. Matter*, vol. 52, pp. 11744–11751, 1995.

[27] D. Sievenpiper, M. Sickmiller, and E. Yablonovitch, "3D wire mesh photonic crystals," *Phys. Rev. Lett.*, vol. 76, pp. 2480–2483, 1996.

[28] J. Pendry, A. Holden, W. Stewart, and I. Youngs, "Extremely low frequency plasmons in metallic mesostructures," *Phys. Rev. Lett.*, vol. 76, pp. 4773–4776, 1996.

[29] V. Kuzmiak, A. Maradudin, and F. Pincemin, "Photonic band structures of two-dimensional systems containing metallic components," *Phys. Rev. B, Condens. Matter*, vol. 50, p. 1683, 1994.

[30] E. Brown and O. McMahon, "Large electromagnetic stop bands in metallodielectric photonic crystals," *Appl. Phys. Lett.*, vol. 67, pp. 2138–2141, 1995.

[31] S. Fan, P. Villeneuve, and J. Joannopoulos, "Large omnidirectional band gaps in metallodielectric photonic crystals," *Phys. Rev. B, Condens. Matter*, vol. 54, pp. 11245–11251, 1996.

[32] S. Gupta, G. Tuttle, and K.-M. Ho, "Infrared filters using metallic photonic band gap structures on flexible substrates," *Appl. Phys. Lett.*, vol. 71, pp. 2412–2415, 1997.

[33] D. Sievenpiper, E. Yablonovitch, J. Winn, S. Fan, P. Villeneuve, and J. Joannopoulos, "3D metallo-dielectric photonic crystals with strong capacitive coupling between metallic islands," *Phys. Rev. Lett.*, vol. 80, pp. 2829–2832, 1998.

[34] G. Kurizki and J. Haus, Eds., *J. Modern Opt. (Special Issue on Photonic Band Structures)*, vol. 41, 1994.

[35] J. Joannopoulos, R. Meade, and J. Winn, *Photonic Crystals: Molding the Flow of Light*. Princeton, NJ: Princeton Univ. Press, 1995.

[36] C. Soukoulis, Ed., *Photonic Band Gap Materials*. Norwell, MA: Kluwer, 1996.
[37] F.-R. Yang, K.-P. Ma, Y. Qian, and T. Itoh "A novel TEM waveguide using uniplanar compact photonic-bandgap (UC-PBG) structure," this issue, pp. 2092-2098.
[38] E. Brown, C. Parker, and E. Yablonovitch, "Radiation properties of a planar antenna on a photonic-crystal substrate," *J. Opt. Soc. Amer. B, Opt. Phys.*, vol. 10, pp. 404–410, 1993.
[39] S. Cheng, R. Biswas, E. Ozbay, S. McCalmont, G. Tuttle, and K.-M. Ho, "Optimized dipole antennas on photonic band gap crystals," *Appl. Phys. Lett.*, vol. 67, pp. 3399–3402, 1995.
[40] E. Brown and O. McMahon, "High zenithal directivity from a dipole antenna on a photonic crystal," *Appl. Phys. Lett.*, vol. 68, pp. 1300–1303, 1996.
[41] M. Kesler, J. Maloney, B. Shirley, and G. Smith, "Antenna design with the use of photonic band-gap materials as all-dielectric planar reflectors," *Microwave Opt. Technol. Lett.*, vol. 11, pp. 169–174, 1996.
[42] M. Sigalas, R. Biswas, Q. Li, D. Crouch, W. Leung, R. Jacobs-Woodbury, B. Lough, S. Nielsen, S. McCalmont, G. Tuttle, and K.-M. Ho, "Dipole antennas on photonic band-gap crystals: Experiment and simulation," *Microwave Opt. Technol. Lett.*, vol. 15, pp. 153–156, 1997.
[43] M. Jensen and Y. Rahmat-Samii, "EM interaction of handset antennas and a human in personal communications," *Proc. IEEE*, vol. 83, pp. 7–17, Jan. 1995.

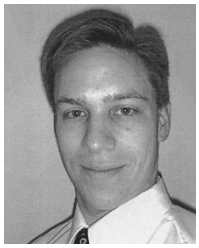

Dan Sievenpiper (S'95–M'98) received the Ph.D. and B.S. degrees in electrical engineering from the University of California at Los Angeles, in 1999 and 1994 respectively.

His research has included photonic crystals, high-impedance electromagnetic surfaces, and novel antennas. He is currently involved in these areas as a Research Staff Member at HRL Laboratories, Malibu, CA.

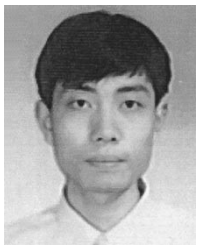

Lijun Zhang was born in Hubei, China, in 1973. He received the B.S. and M.S. degrees from the University of Science and Technology of China, Hefei, China, in 1993 and 1996, respectively, and is currently working toward the Ph.D. degree at the University of California at Los Angeles.

His recent research activities have focused on the numerical modeling of novel PBG materials and their applications in printed antennas, antenna arrays, and FSS's.

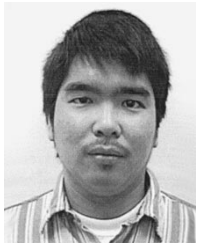

Romulo F. Jimenez Broas was born in Cavite, Philippines, on September 23, 1975. He received the A.B. degree in physics from the University of California at Berkeley, in 1996, and is currently working toward the M.Sc. degree in electrical engineering from the University of California at Los Angeles.

From 1997 to 1998, he was a Member of the Technical Staff at the TRW Antenna Products Center, where he performed computer simulations and analysis of multibeam antenna systems and architectures.

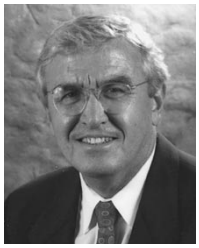

Nicolaos G. Alexópoulos (S'68–M'69–SM'82–F'87) was born in Athens, Greece, on April 14, 1942. He received the degree from the Eighth Gymnasium of Athens, Athens, Greece in 1959, and the B.S.E.E., M.S.E.E., and Ph.D. degrees from The University of Michigan at Ann Arbor, in 1965, 1967, and 1968, respectively.

From 1969 to 1996, he joined the School of Engineering and Applied Science, University of California at Los Angeles (UCLA), where he was a member of the faculty of the Electrical Engineering Department. While with UCLA, he served as Associate Dean for Faculty Affairs (1986–1987) and Chair of the Electrical Engineering Department (1987–1992). Since January 1997, he has been a Professor in the Electrical and Computer Engineering Department, University of California at Irvine, where he also serves as the Dean of the School of Engineering. He has served over the years as a Consultant to a variety of U.S. and foreign corporations and the U.S. Government. In addition, he has been on the editorial board of various professional journals and, more recently, he served as the Editor-in-Chief of *Electromagnetics*. He has authored over 250 refereed journal and conference proceedings papers. His recent research activities have focused on the modeling and design of three-dimensional integrated circuits and printed antennas in multilayered materials, wireless communication antennas and systems, interconnect problems in complex networks, novel materials and smart structures in low observable systems, and computational methods.

Dr. Alexopoulos was co-recipient of the IEEE S. E. Schelkunoff Prize Best Paper Award in both 1985 and 1998.

Eli Yablonovitch (M'75–SM'90–F'92) received the Ph.D. degree in applied physics from Harvard University, Cambridge, MA, in 1972.

He was with Bell Telephone Laboratories for two years, and then became a Professor of applied physics at Harvard University. In 1979, he joined the Exxon Corporation to perform research on photovoltaic solar energy. In 1984, he joined Bell Communications Research, where he was a Distinguished Member of Staff, and also Director of Solid-State Physics Research. In 1992, he joined the University of California at Los Angeles (UCLA), where he is Professor of electrical and engineering and Director of the UCLA Nanoelectronics Laboratory. His work has covered a broad variety of topics, including nonlinear optics, laser–plasma interaction, infrared laser chemistry, photovoltaic energy conversion, strained-quantum-well lasers, and chemical modification of semiconductor surfaces. His current main interests are in optoelectronics, high-speed optical communications, high-efficiency light-emitting diodes and nanocavity lasers, photonic crystals at optical and microwave frequencies, quantum computing, and quantum communication.

Dr. Yablonovitch is a Fellow of the American Physical Society and the Optical Society of America, and is a member of Eta Kappa Nu. He chaired the 1979 Gordon Conference on Nonlinear Optics and Lasers. He has been the recipient of numerous honors and awards, including an Alfred P. Sloan Fellowship (1978–1979), the Adolf Lomb Medal of the Optical Society of America (1978), an R&D 100 Award (1990) the W. Streifer Scientific Achievement Award presented by the IEEE Lasers and Electro-Optics Society (LEOS) (1993), and the R. W. Wood Prize of the Optical Society of America (1996).